Disoriented chiral condensate dynamics in the $(2+1)$D $O(3)$ model

G. Holzwarth*
Fachbereich Physik, Universität Siegen, D-57068 Siegen, Germany
(Received 18 July 2001; published 30 January 2002)

The dynamics of symmetry breaking after a quench is numerically simulated on a lattice for the $(2+1)$-dimensional $O(3)$ model. In addition to the standard sigma model with a temperature-dependent Φ^4 potential the energy functional includes a four-derivative current-current coupling to stabilize the size of the emerging extended topological textures. The total winding number can be conserved by constraint. As a model for the chiral phase transition during the cooling phase after a hadronic collision this allows us to investigate the interference of ''baryon-antibaryon'' production with the developing disoriented aligned domains. The growth of angular correlations, condensate, and average orientation is studied in dependence of texture size, quench rate, and symmetry breaking. The classical dissipative dynamics determines the rate of energy emitted from the relaxing source for each component of the 3-vector field which provides a possible signature for the domains of disoriented chiral condensate (DCC). We find that the ''pions'' are emitted in two distinct pulses; for sufficiently small lattice size the second one carries the DCC signal, but it is strongly suppressed as compared to simultaneous ''sigma''-meson emission. We compare the resulting anomalies in the distributions of DCC pions with probabilities derived within the commonly used coherent state formalism.

DOI: 10.1103/PhysRevD.65.054013 PACS number(s): 12.39.Fe, 11.27.+d, 12.39.Dc, 25.75.−q

I. INTRODUCTION

The observation of clear signatures for the chiral phase transition still remains one of the outstanding challenges of hadron physics. There is hope that the extreme energy densities located inside the spatial region between receding baryonic slabs shortly after ultrarelativistic baryon or heavy-ion collision may provide physical conditions for such a phase transition to take place.

From the theoretical point of view we are dealing with a complex dynamical system, strongly interacting quantum fields with many different fermionic and bosonic degrees of freedom, far from equilibrium, creating and emitting baryons and mesons from a rapidly expanding and cooling spatial volume. Correspondingly, there is a vast theoretical literature ranging from cascade models in the colored partonic degrees of freedom to hydrodynamic flow models for hadronic currents, which might be applicable at different stages and might shed light on different aspects during the time evolution of such events. If within the hot fireball chiral symmetry is indeed restored then the dynamics of its spontaneous breaking and formation of a chiral condensate is one important aspect of the cooling process in which the highly excited spatial volume returns back to the normal physical vacuum.

A possible strategy that has proven useful for many other cases of phase transitions in microscopically very complex systems is to comprise the essential phenomenology into an effective action for an ordering parameter field. For the hadron phenomenology near $T=0$ a chiral field with spontaneously broken $O(4)$ symmetry has become a standard and successful tool, so it is natural to try to extend and apply this concept to the temperature region where the chiral phase transition is expected. In its most simple version the effective action then consists of the $(3+1)$dimensional $O(4)$ linear σ model, with a suitable temperature-dependent Φ^4 potential for the spontaneous symmetry breaking. Depending on the ratio between relaxation and cooling times, the dynamics of the ordering field then follows the cooling quench imposed on the temperature dependence of the potential. As in other cases of multicomponent field ordering, it is characterized by the formation and growth of misaligned domains separated by domain walls or other topologically nontrivial structures, depending on field and space dimensionality [1]. Numerical simulations in this classical framework have been performed and they confirm the transient formation of domains of false vacuum, in which the condensate is approaching its vacuum value while the direction of the aligned field still deviates from the surrounding vacuum [2]. The possible influence of quantum- and thermal effects has been investigated, mostly in mean-field approximation [3]. It has been suggested that pions emitted from these domains of disoriented chiral condensate (DCC) carry the misalignment in their isospin multiplicities, and in this way may provide a signature of the phase transition [4].

A peculiar feature of the chiral $O(4)$ field in three spatial dimensions is that its winding density may be identified with baryon density [5]. This has led to a most interesting and remarkably successful model for baryon structure and dynamics at $T=0$. The corresponding topological arguments [6] have been used [7] to estimate nascent baryon-antibaryon multiplicities in random chiral field configurations at high temperature; of course, the first few time steps in an ordering evolution lead to an almost instantaneous reduction of the initially large and rapidly fluctuating winding densities.

Strictly, the topological conservation of the total winding number is limited to a field manifold where the point $\Phi=0$ is excluded. In numerical simulations of field evolutions on a discrete spatial lattice, however, even topological conservation laws have to be enforced by constraint, because arguments based on continuity cannot be applied. Therefore there is no principal difference for implementing on a lattice the

*Email address: holzwarth@physik.uni-siegen.de

conservation of a winding number in the nonlinear or linear realization of the $O(4)$ symmetry. This allows us to study the formation of the condensate and disoriented domains during the phase transition with simultaneously forming baryons plus antibaryons such that the total baryon number is fixed to any desired value. It is well known that topological textures play an important role in ordering transitions, so it is of special interest to study how the stabilization of extended baryonic structures and baryon number conservation may affect the growth laws of DCC domains, and possible DCC signatures in the emitted radiation. For this purpose it is necessary to include in the effective action terms which stabilize the spatial size of the baryons generated in the course of the ordering evolution. Scaling arguments show that an additional four-derivative term is sufficient for soliton stabilization in 2- and 3-dimensional $O(n)$ models. A different extension, the inclusion of the anomaly term, has been advocated to increase the probability of DCC-formation [8].

The linear σ-model (even with explicite inclusion of quarks) sometimes has been used [9] to investigate the possibility of DCC-signals by considering spatially averaged fields, only. Naturally, within such an approximation the effects we are investigating here, are lost. On the other hand, there is no immediate need to explicitly include fermionic degrees of freedom in our present approach.

Before embarking on a full-scale simulation of the $(3+1)$-dimensional $O(4)$ case it is helpful to analyze the relevant questions in the $(2+1)$-dimensional $O(3)$ model [10]. It shares all essentials with the higher-dimensional case. Although it represents an efficient tool for the description of 2-dimensional spin systems in its own right [11], we here discuss it mainly in view of its hadron physics generalization. That is, we denote the order parameter field as a ''chiral'' meson field. We call the fluctuations ''pions'' with internal ''isospin'' components, and σ mesons, which aquire mass through spontaneous breaking of the chiral $O(3)$ symmetry, and we call the domains with small values of the condensate and unbroken symmetry ''bags,'' in which the ''baryonic'' winding density is confined. Although there is no compelling connection to fix the parameters of the model from its higher-dimensional analogue, we choose them in correspondence to simulate relative sizes and masses for baryons and mesons. Various features of the static solutions of this model, and their formation in relaxation processes after a quench, have been studied in [12,13]. In the present investigation we discuss in more detail the different stages which characterize the long-time ordering evolution under dissipative dynamics, the dependence of the relevant times on model parameters, different types of symmetry breaking, and quench rates. Our main aim, however, is an attempt to extract from the dynamics of the evolution the possibility of a DCC signal. Generally, the emission of radiation from a moving source is determined by quantum-field-theoretic amplitudes which require a separation of the time-dependent field into a classically moving part and quantum fluctuations. The result is commonly put into the statement that the ''intensity of pion radiation is proportional to the square of the classical pion field'' [4]. This argument is the basis of the interest in DCC pions. We analyze the validity of this statement under the assumption of dissipative dynamics, i.e., assuming that the energy loss of the relaxing and ordering classical configurations is carried away by propagating fluctuations. Under this assumption we obtain the timing and strength and isospin distribution of DCC pions from purely classical considerations.

This general dynamical scheme is outlined in Sec. II, while the specifics of the model and the observables of interest are defined in Sec. III. The essential features of configurations during the course of the transition, the growth of angular correlations, a decrease of the numbers of textures, the saturation of the condensate and average orientation, and the formation of baryonic clusters, are presented in Secs. IV, V, and VI with a dependence on parameters of the model, symmetry breaking, and cooling rates. Finally, in Sec. VII, we analyze the rates of energy loss with respect to possible DCC pion pulses, and we extract the isospin distributions from large ensembles of events. Conclusions are drawn in Sec. VIII.

II. NONEQUILIBRIUM FIELD DYNAMICS AND DCC SIGNALS

We consider an effective action for an $O(3)$ vector field $\mathbf{\Phi}$:

$$\mathcal{S}[\mathbf{\Phi}]=\int (\mathcal{T}[\mathbf{\Phi}]-\mathcal{U}[\mathbf{\Phi}])d^2xdt \tag{1}$$

where the kinetic energy density $\mathcal{T}[\mathbf{\Phi}]$ comprises all terms containing time derivatives of $\mathbf{\Phi}$. We consider the evolution of field configurations, which at some initial time deviate from the global equilibrium configuration (the ''true vacuum'') within some finite spatial region V. The equations of motion $\delta\mathcal{S}/\delta\mathbf{\Phi}=0$ which govern the classical evolution of the initial non-equilibrium configuration describe both, the approach towards the vacuum configuration in the interior of that spatial region and the propagation of outgoing (distorted) waves into the (initially undisturbed) surrounding vacuum. Although, of course, the classical equations of motion conserve the total energy $E=\int(\mathcal{T}+\mathcal{U})d^2x$, the outgoing waves carry away energy from the interior of the spatial region in which the total energy $E=T+U$ initially was located.

In quantum field theory the quantization of the propagating fluctuations describes multiparticle production of pions emitted from the relaxing field configurations. In a separation

$$\mathbf{\Phi}(\boldsymbol{x},t)=\mathbf{\Phi}_{cl}(\boldsymbol{x},t)+\delta\mathbf{\Phi}(\boldsymbol{x},t) \tag{2}$$

where $\mathbf{\Phi}_{cl}$ comprises all of the large amplitude motion of $\mathbf{\Phi}$ and $\delta\mathbf{\Phi}$ contains only small fluctuations around $\mathbf{\Phi}_{cl}$, the expansion of $\mathcal{S}[\mathbf{\Phi}]$ to second order in $\delta\mathbf{\Phi}$

$$\mathcal{S}[\mathbf{\Phi}]=\mathcal{S}[\mathbf{\Phi}_{cl}]+\int \left.\frac{\delta\mathcal{S}}{\delta\mathbf{\Phi}(\boldsymbol{x}',t')}\right|_{[\mathbf{\Phi}_{cl}]}\delta\mathbf{\Phi}(\boldsymbol{x}',t')d^2x'dt' + \int\int \delta\mathbf{\Phi}(\boldsymbol{x}',t')\left.\frac{\delta^2\mathcal{S}}{\delta\mathbf{\Phi}(\boldsymbol{x}',t')\,\delta\mathbf{\Phi}(\boldsymbol{x}'',t'')}\right|_{[\mathbf{\Phi}_{cl}]} \times\delta\mathbf{\Phi}(\boldsymbol{x}'',t'')d^2x'dt'd^2x''dt''+\mathcal{O}(\delta\Phi^3) \tag{3}$$

and variation with respect to $\delta\mathbf{\Phi}$ provides the classical expression for the fluctuating part

$$\delta\mathbf{\Phi}(\boldsymbol{x},t)=\delta\mathbf{\Phi}^{(0)}(\boldsymbol{x},t) + \int \mathcal{G}(\boldsymbol{x},t,\boldsymbol{x}',t')\left.\frac{\delta\mathcal{S}}{\delta\mathbf{\Phi}(\boldsymbol{x}',t')}\right|_{[\mathbf{\Phi}_{cl}]}d^2x'dt'. \tag{4}$$

The homogeneous part $\delta\mathbf{\Phi}^{(0)}$, after quantization, represents the scattering of field quanta off the classical configuration $\mathbf{\Phi}_{cl}$ (i.e., these are on-shell distorted waves). The Green's function $\mathcal{G}(\boldsymbol{x},t,\boldsymbol{x}',t')$ of the operator $\delta^2\mathcal{S}/(\delta\mathbf{\Phi}\delta\mathbf{\Phi})|_{[\mathbf{\Phi}_{cl}]}$ relates emitted (i.e. on-shell) radiation to the source term $\delta\mathcal{S}/\delta\mathbf{\Phi}|_{[\mathbf{\Phi}_{cl}]}$. There is, however, no unique way to separate the propagating fluctuations $\delta\mathbf{\Phi}$ from a more or less smoothly evolving classical configuration $\mathbf{\Phi}_{cl}$ because both $\mathbf{\Phi}_{cl}$ and $\delta\mathbf{\Phi}$, are integral parts of one and the same evolving order-parameter field $\mathbf{\Phi}$. Conclusions drawn from one part only are subject to the arbitrariness of the chosen separation. In any case, in an equation of motion that separately describes the evolution of $\mathbf{\Phi}_{cl}$ we expect a dissipative term to account for the loss of energy through the emitted radiation:

$$\frac{1}{\tau}\dot{\mathbf{\Phi}}_{cl}=\delta\mathcal{S}/\delta\mathbf{\Phi}|_{[\mathbf{\Phi}_{cl}]}. \tag{5}$$

For sufficiently small values of the relaxation constant τ the dissipative term dominates the time evolution of $\mathbf{\Phi}_{cl}$, propagating parts get damped away and we can replace Eq. (5) by the time-dependent Ginzburg-Landau (TDGL) equation

$$\frac{1}{\tau}\dot{\mathbf{\Phi}}_{cl}=-\delta U/\delta\mathbf{\Phi}|_{[\mathbf{\Phi}_{cl}]}. \tag{6}$$

The potential energy functional U contains no time derivatives of $\mathbf{\Phi}$, therefore $\mathbf{\Phi}_{cl}$ has no propagating parts, i.e. it does not pick up field momentum, and it provides a very slowly moving adiabatically evolving classical background field.

Back reaction of the fluctuations on the moving classical field can re-enter in different ways: as loop corrections they can lead to renormalization of the coupling constants in the functional U which thus may become time or temperature dependent and drive the spontaneous symmetry breaking; an appropriate noise term to be added on the right-hand side of Eq. (6) accounts for stochastic interactions of the fluctuations with $\mathbf{\Phi}_{cl}$ at finite temperature. Ideally, through that procedure one hopes to achieve a separation (2) such that the fluctuating parts $\delta\mathbf{\Phi}$ contain no exponentially increasing amplitudes during the relaxation process.

In the following we assume that the coupling constants which appear in the TDGL-equations have their renormalized physical values with an appropriate time or temperature dependence and we will restrict the discussion to the consequences of those equations. Evolutions via Eq. (6) of individual initial $\mathbf{\Phi}_{cl}$ configurations into final quasi-stable configurations are denoted as ''events,'' and we shall consider ensembles of events sampled with different initial configurations. The individual events show a variety of physically interesting features, textures, walls, disoriented domains, and growth laws, which form the main body of the subsequent discussions. The lack of second-order time derivatives in Eq. (6) means that also localized stable structures created in $\mathbf{\Phi}_{cl}$ will not propagate but only drift in response to their mutual interaction. This is as expected because uniform motion of textures represents zero modes which may still be contained in $\delta\Phi$. With Eq. (6) the rate of decrease of the energy $U_{cl}=U[\mathbf{\Phi}_{cl}]$ stored in the classical configuration $\mathbf{\Phi}_{cl}$ then is

$$\dot{U}_{cl}(t)=-\frac{1}{\tau}\int|\dot{\mathbf{\Phi}}_{cl}(\boldsymbol{x},t)|^2d^2x. \tag{7}$$

If particle emission from the evolving source is the only mechanism for energy nonconservation this rate of energy loss has to match the energy flow carried away by the emitted radiation. This requirement determines the relaxation constant τ in Eq. (6) which fixes the time scale for the approach of $\mathbf{\Phi}_{cl}$ towards equilibrium. (Of course, external interference with the system like Bjorken rescaling of the spatial metric may provide other sources of energy nonconservation.)

In quantum field theory, for field fluctuations coupled to a time-dependent classical source $s(\boldsymbol{x},t)$, the probability density for the emission of $n_{\boldsymbol{k}}$ field quanta with momentum $\boldsymbol{k}$ and mass m is given by

$$n_{\boldsymbol{k}}=|s(\boldsymbol{k},\omega_k)|^2/(2\omega_k) \tag{8}$$

where $s(\boldsymbol{k},\omega_k)$ is the energy-momentum-space transform of the source, expanded in terms of the complete set of distorted scattering states with asymptotic momentum $\boldsymbol{k}$, and taken at the on-shell energy $\omega=\omega_k=\sqrt{k^2+m^2}$.

In our present case according to Eq. (4) the time-dependent source is given by $\delta\mathcal{S}/\delta\mathbf{\Phi}|_{[\mathbf{\Phi}_{cl}(\boldsymbol{x},t)]}$. Consistent with our assumptions about the slow motion of the classical field $\mathbf{\Phi}_{cl}$ we again may approximate here $\delta\mathcal{S}/\delta\mathbf{\Phi}$ by $-\delta\mathcal{U}/\delta\mathbf{\Phi}$. With $\mathbf{\Phi}_{cl}$ obeying the TDGL equations (6) the source field then is just the time derivative of the classical field $\dot{\mathbf{\Phi}}_{cl}(\boldsymbol{x},t)/\tau$ and we obtain for the average number of particles emitted with momentum $\boldsymbol{k}$ and isospin component i (omitting the index cl):

$$n_{i,\boldsymbol{k}}=\frac{|\dot{\mathbf{\Phi}}_i(\boldsymbol{k},\omega_k)/\tau|^2}{2\omega_k}. \tag{9}$$

With particle emission as the only mechanism for energy nonconservation the total energy $\Delta E=\int \omega_k \Sigma_i n_{i,\boldsymbol{k}} d^2k$ carried away by radiation during the ordering process must balance the loss of energy stored in the classical field. With Eq. (7) this requirement leads to

$$\frac{1}{2}\int |\dot{\boldsymbol{\Phi}}_{cl}(\boldsymbol{k},\omega_k)|^2 d^2k = \tau \int |\dot{\boldsymbol{\Phi}}_{cl}(\boldsymbol{x},t)|^2 d^2x dt. \qquad (10)$$

Note that on the left-hand side of this equation only on-shell frequencies appear, while the right-hand side (when written in Fourier space) contains an independent integral over all Fourier components of the moving classical field. Of course, together with Eq. (6), this relation is an implicit definition of the relaxation constant τ.

For the adiabatically evolving process we consider the time t as a parameter such that we may define

$$\epsilon_i(t)=\frac{1}{\tau}\int \dot{\Phi}_i(\boldsymbol{x},t)^2 d^2x = \frac{L^2}{\tau}\langle \dot{\Phi}_i^2(t)\rangle \qquad (11)$$

as the energy carried away per time interval by particles emitted with field orientation i. Here "$\langle\ \rangle$" denotes the lattice average over an $L\times L$ lattice. Due to the slow motion of the source we expect the particles to be mainly emitted with low energies, i.e. with low momenta $k\approx 0$ and $\omega_i \approx m_i$. In our present context we choose the $O(3)$ symmetry to be spontaneously broken in 3-direction (selected by the surrounding true vacuum boundary condition or by small explicit symmetry breaking, or by a small bias in the initial configuration). Then the $i=1,2$ ("isospin") components of the $O(3)$ chiral field constitute two "pionic" fluctuational fields $\delta\Phi_i=\pi_i$ with small mass $m_{1,2}=m_\pi$ due to explicit symmetry breaking, while the σ fluctuation $\delta\Phi_3$ acquires a large mass m_σ due to the spontaneously broken symmetry. So we expect the emission rate for pions with isospin component $i=1,2$:

$$n_i(t)=\frac{\epsilon_i(t)}{m_\pi}. \qquad (12)$$

During the early stages of the ordering evolution the spatial averages $\langle \dot{\Phi}_i^2(t)\rangle$ will be similar for both isospin directions, but at late times with the formation of larger disoriented domains they might differ appreciably. The relative abundancies

$$f_i(t)=\frac{n_i(t)}{n_1(t)+n_2(t)} \qquad (13)$$

are free of unknown constants and could serve as the DCC signature, if it is possible to separate in each individual event the small number of late time pions from the background of those produced during earlier stages, from decaying σ's, and from other sources.

III. THE MODEL

The features which are of physical interest in the chiral phase transition for a cooling hadronic gas in the $(3+1)$-dimensional $O(4)$ model can be explored and demonstrated in the lower-dimensional $O(3)$ model. It is defined in terms of the dimensionless 3-component field $\boldsymbol{\Phi}=\Phi\hat{\boldsymbol{\Phi}}$ with $\hat{\boldsymbol{\Phi}}\cdot\hat{\boldsymbol{\Phi}}=1$, with the following Lagrangian density in $2+1$ dimensions:

$$\mathcal{L}=\frac{1}{2}\partial_\mu\boldsymbol{\Phi}\partial^\mu\boldsymbol{\Phi}-\frac{\lambda}{4l^2}(\Phi^4-2f^2\Phi^2+1)-\lambda l^2\rho_\mu\rho^\mu+m_\pi^2\Phi_3. \qquad (14)$$

In addition to the usual linear sigma model with a standard Φ^4 potential for the modulus field Φ, this Lagrangian contains a four-derivative current-current coupling $\rho_\mu\rho^\mu$ for the conserved topological current

$$\rho^\mu=\frac{1}{8\pi}\epsilon^{\mu\nu\rho}\hat{\boldsymbol{\Phi}}\cdot(\partial_\nu\hat{\boldsymbol{\Phi}}\times\partial_\rho\hat{\boldsymbol{\Phi}}), \qquad (15)$$

which satisfies $\partial_\mu\rho^\mu=0$. In the present $O(3)$ model this nonlinear coupling comprises the four-derivative "Skyrme" term and the sixth-order current-current coupling of effective chiral $O(4)$ models.

The independent strengths of the Φ^4 and the Skyrme couplings are written in terms of one common dimensionless parameter λ and a length l which may be absorbed into the space-time coordinates. So, for λ fixed, l sets the scale for the spatial extent of localized static solutions, in lattice implementations relative to the size of the basic lattice unit cell. The static solutions have been investigated and described in [12]. For continuous coordinates (or, on a lattice, for $l\gg 1$) the total energy (apart from the explicitly symmetry-breaking m_π^2 contribution) of such localized solutions is independent of l (as long as l is small as compared to the total lattice size L). In the following we put the lattice constant to unity.

If we consider the field $\boldsymbol{\Phi}$ as the basic order parameter to reflect the chiral phase transition as function of the temperature T, then the factor f^2 which multiplies the square of the field vector in Eq. (14) drives the spontaneous symmetry breaking. As the temperature goes to zero it is supposed to converge towards its vacuum value $f^2(T\to 0)\to 1$, and it should become very small $f^2(T\to T_c)\ll 1$ as T approaches the critical temperature T_c. For very high temperature $f^2(T>T_c)$ is supposed to become negative.

A small symmetry-breaking term with strength m_π^2 has also been added to the otherwise $O(3)$-symmetric Lagrangian (14). This explicit symmetry breaking is applied in 3-direction of the internal space. If unequal zero it singles out the 3-component Φ_3 of the $\boldsymbol{\Phi}$ field as that field which aquires the nonvanishing condensate at $T=0$, and we will denote this component as the "σ" field, while the 1- and 2-components represent the "pionic" (Goldstone) degrees of freedom of the remaining unbroken symmetry.

It is convenient to have also for nonvanishing m_π^2 the minimum of the $(T=0)$ potential located at the vacuum field configuration $\mathbf{\Phi}=(0,0,1)$, such that the length Φ of the field vectors approaches unity for $T=0$ also for nonzero symmetry breaking. This is achieved by subtracting $m_\pi^2 l^2/\lambda$ from f^2 in the coefficient of the second order term in the potential $V(\Phi)$ in Eq. (14)

$$f^2 = f^2(T) - \frac{m_\pi^2 l^2}{\lambda}. \tag{16}$$

This form shows directly how the explicit symmetry breaking supplies the pionic Goldstone bosons with mass m_π. For $T<T_c$ the temperature dependence of m_π^2 can be ignored. On the other hand, the mass of the σ field is given by

$$m_\sigma^2 = 2\frac{\lambda}{l^2} f^2(T) + m_\pi^2 \tag{17}$$

which is mainly determined by the temperature dependence of $f^2(T)$.

Evolution of $\mathbf{\Phi}_{cl}$ proceeds through the TDGL equations of motion as they result from the potential part of Eq. (14) (i.e. also from the current-current coupling only the density term ρ_0^2 is kept). As no other time-derivative terms appear on the right-hand side, the constant τ which multiplies the left-hand side of Eq. (6) can be set to one, i.e. in the following the relaxation time τ serves as the time unit. Omitting for convenience the index "cl" we have

$$\frac{1}{\tau}\dot{\Phi}_i = \Delta\Phi_i - \frac{\lambda}{l^2}(\Phi^2 - f^2)\Phi_i - \lambda l^2 \frac{\delta(\rho_0^2)}{\delta\Phi_i} + m_\pi^2 \delta_{i3} + \xi_i . \tag{18}$$

As far as the dissipative term originates from the elimination of fluctuational modes which simulate a heat bath for the evolving field configuration, the addition of fluctuational noise $\boldsymbol{\xi}$ is required with a strength dictated by the dissipation-fluctuation theorem. Such a term has also been added in Eq. (18).

In lattice implementation, we impose periodic boundary conditions on the field configurations. This implies compactification of coordinate space to a torus $S^1 \times S^1$. These boundary conditions preserve the global $O(3)$ symmetry of the model (for vanishing m_π^2). Having singled out the 3-direction as the σ direction in which the $T=0$ condensate is formed, we can impose the stronger vacuum boundary conditions $\mathbf{\Phi}=(0,0,1)$ for all points on the lattice boundary throughout the whole evolution. This implies compactification of coordinate space to the two-sphere S^2. In both cases the winding density ρ_0 satisfies $\int \rho_0 d^2x = B$ with integer winding number B. Of course, these vacuum boundary conditions represent another way of explicit symmetry breaking which eventually drives the evolution of the condensate into the 3-direction. It is, however, a very weak form which is only active at the surface of the spatial region, unlike a nonvanishing m_π^2 term which is locally active at every point in space.

With the equations of motion (18) being purely first order in time derivatives it is sufficient to specify for initial conditions at $t=0$ only the field configurations themselves. As the time-dependent fluctuations are not part of $\mathbf{\Phi}_{cl}$ the high-temperature initial configuration is (apart from a small optional bias in 3-direction due to an explicit symmetry breaker), $\mathbf{\Phi}_{cl} \equiv 0$ in the interior of the spatial region in which the hot chiral field is located and takes the true vacuum values on its boundary. The first step in the time evolution is therefore governed by the stochastic force $\boldsymbol{\xi}$ alone. But this first step will immediately create a configuration $\mathbf{\Phi}_{cl}$ which is of a stochastic nature itself. Therefore, choosing each of the three Cartesian field components at each interior point of the lattice from a random Gaussian deviate, and fixing $\mathbf{\Phi}_{cl} = (0,0,1)$ on the boundary of the lattice, provides convenient initial configurations with initial spatial correlation length less than one lattice unit. From these random configurations, those with the desired total winding number B are selected and propagated in time. During the evolution of each individual event the fluctuational noise $\boldsymbol{\xi}$ at every time step and every lattice point is picked from an appropriate Gaussian deviate. A large number of events generated in this way constitute the statistical ensemble from which ensemble averages can be obtained at some point in time during the evolution.

For configurations where the orientation of the vector field $\mathbf{\Phi}$ shows strong local variations (as happens near localized textures or throughout random initial distributions) the implementation of the winding density ρ_0 on the lattice in the differential form (15) is not sufficiently accurate to add up to the integer total winding number B. Therefore ρ_0 and its functional derivatives have to be evaluated according to the geometrical meaning of ρ_0 as the surface area of spherical triangles cut out on the two-sphere S^2 by the image of elementary triangles in coordinate space. Details of this procedure have been discussed in [13]. It allows us to assign a value $\rho(i,j)$ of the winding density ρ_0 to each point (i,j) of the square lattice [or, more precisely, to each lattice cell with the lower left corner (i,j)] such that the total winding number

$$B = \sum_{i,j=0}^{L-1} \rho(i,j) \tag{19}$$

summed over the whole lattice is an integer and initial configurations can be selected with some desired integer value of B. We also define

$$D = \sum_{i,j=0}^{L-1} |\rho(i,j)| \tag{20}$$

by summing up the absolute values of the local winding densities. Of course, for random or slowly varying smooth configurations D generally is not an integer. However, if a configuration describes a distribution of localized textures (and antitextures) which are sufficiently well separated from each other, then D is close to an integer and counts the num-

ber of these textures (plus antitextures). In that case we can define the numbers N_+, N_- of ''particles'' and ''antiparticles'' through

$$B = N_+ - N_-, \quad D = N_+ + N_-. \tag{21}$$

In the following we will briefly call D the ''particle number,'' even if it is not integer and comprises textures and antitextures.

In a lattice implementation the local update of $\mathbf{\Phi}(i,j)$ at some time step at some lattice point (i,j) will occasionally lead to a discrete jump in the total winding number B. For well-developed localized structures this corresponds to unwinding textures or antitextures independently, such that B decreases or increases by one or more units. This will eventually happen even for implementations of the nonlinear $O(3)$ model where the length Φ is constrained to unity and B is topologically conserved, because the topological arguments based on continuity do not apply to the discrete lattice configurations. It can be prevented by an (optional) B filter which rejects such a B-violating local field update at that lattice point and time step. This eliminates all independent unwinding processes. Only simultaneous annihilation of texture and antitexture in the same time step remains possible, and, as the update proceeds locally at each lattice vertex it can happen only if texture and antitexture overlap. This B-conserving evolution is characteristic for the nontrivial topology of the nonlinear $O(3)$ model and in this way can be implemented as an optional constraint also into the linear $O(3)$ model. In the continuum limit it implies that a vanishing modulus $\Phi = 0$ of the field vector is excluded.

IV. ROLL DOWN AND DOMAIN GROWTH AFTER SUDDEN QUENCH

In order to get a feeling for a reasonable choice of the two essential parameters l and λ in Eq. (14) we study at first the simple case of a sudden quench without any symmetry breaking, neither explicit nor via boundary condition, the so-called critical quench. That is, we put $m_\pi^2 = 0$ and impose only periodicity for otherwise arbitrary field vectors at the boundary of a sufficiently large $L \times L$ lattice. The sudden quench is realized by exposing the initially (at $t=0$) random configuration to the $T=0$ value of $f^2(T=0) \equiv 1$ for all times $t>0$. For this zero-temperature evolution the noise term $\boldsymbol{\xi}$ is also not present. As an example Fig. 1 shows one individual evolution of a configuration with fixed winding number $B=0$, on a lattice with $L=150$, with $l=2$ and $\lambda=1$.

As significant observables we show the time dependence of total energy E, particle number D, field modulus $\langle\Phi\rangle$ averaged over the whole lattice, and the angular correlation length R_D. The latter is defined as the (interpolated) half-maximum distance $R_{1/2}$ of the equal-time angular correlation function

$$C(R) = \sum_{i,j=0}^{L} \sum_{k,l=0}^{L} \hat{\mathbf{\Phi}}(i,j) \cdot \hat{\mathbf{\Phi}}(k,l) \Big/ \sum_{i,j=0}^{L} \sum_{k,l=0}^{L} 1 \tag{22}$$

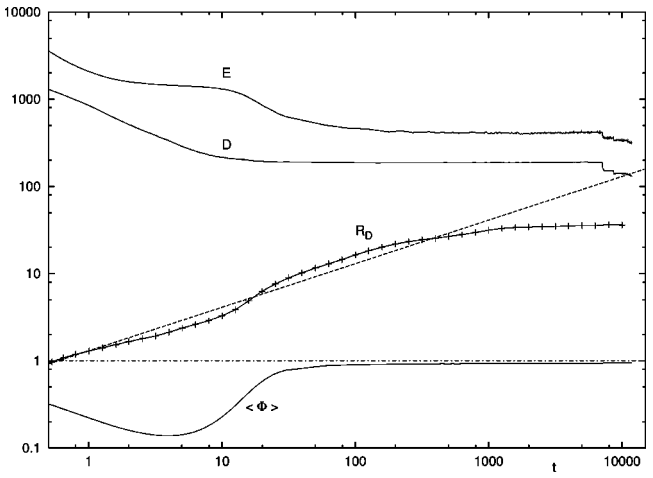

FIG. 1. Total energy E, particle number D, angular correlation length R_D, and the average length of the field vector $\langle\Phi\rangle$ as functions of time after a sudden quench (for $l=2$, $\lambda=1$). The total winding number is $B=0$ by constraint throughout the evolution. The dashed line indicates the classical growth law $R_D \sim t^{0.5}$.

[with the k,l sum restricted such that the distance $r = \sqrt{(k-i)^2+(l-j)^2}$ between lattice vertices (i,j) and (k,l) lies inside bins of unit size around fixed positive integers R]. Note that the definition (22) contains only the unit vectors $\hat{\mathbf{\Phi}}$, and not the full field vectors $\mathbf{\Phi}$, i.e. $C(R)$ measures only the angular correlations in a given configuration. As discussed in [13] this definition of R_D serves well to provide an average radius of oriented domains.

Figure 1 follows the evolution over a very long time (up to $t \sim 10^4$ relaxation-time units) and clearly shows the different phases of the ordering process. Up to $t \sim 10$ the average $\langle\Phi\rangle$ stays (or becomes) small (~ 0.1), while the particle number D decreases by almost one order of magnitude due to local angular reorientation, also reflected in R_D which increases approximately as $t^{0.4}$. Once the oriented domains have reached sizes which cover several lattice units the roll-down phase sets in where Φ approaches unity within these domains (while remaining small at their boundaries where strong angular variations prevail). This roll-down phase takes a few tens of time units and it is accompanied by a significant energy reduction and a more rapid increase of R_D, such that by the end of this roll down the oriented domains cover areas with typical radii of 10 lattice units. During the end of and after this phase the isolated textures assume their stable shapes with the appropriate bag and angular field profiles. This is accompanied by further angular ordering of the topologically trivial field configurations in which these textures are embedded, which proceeds by moving boundaries between differently oriented domains. It leads to a further decrease of E and an increase of R_D, which follows very nicely the classical $t^{0.5}$ Allen-Cahn law [14]. This phase lasts up to several hundreds of time units, without further reduction of the particle number D. Because of the existence of the remaining stable bags the average Φ does not reach the vacuum limit $\langle\Phi\rangle = 1$ and due to the floating angular textures the increase in R_D begins to saturate after $t \sim 10^3$. On a time scale which is still larger by another order of magnitude the

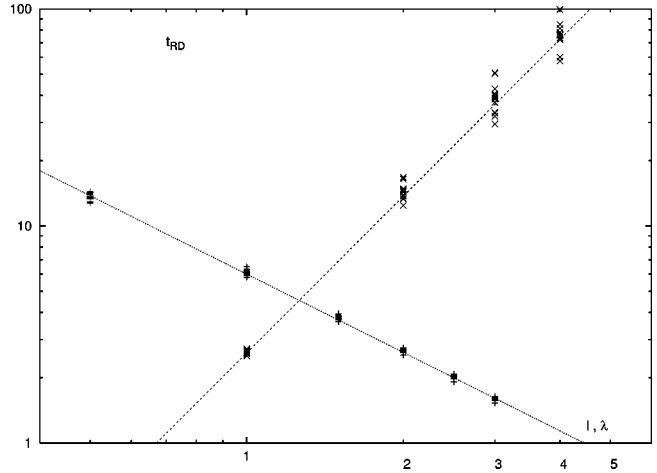

FIG. 2. The roll-down time t_{RD} for different values of the scale l (with coupling constant $\lambda=2$), and different values of λ (with scale $l=1$), respectively. For each set of parameters 15 events ($B=0$) on a 120×120 grid are sampled. The straight lines indicate the power laws $t_{RD}=2.6l^{2.4}$ and $t_{RD}=6\lambda^{-1.2}$, respectively.

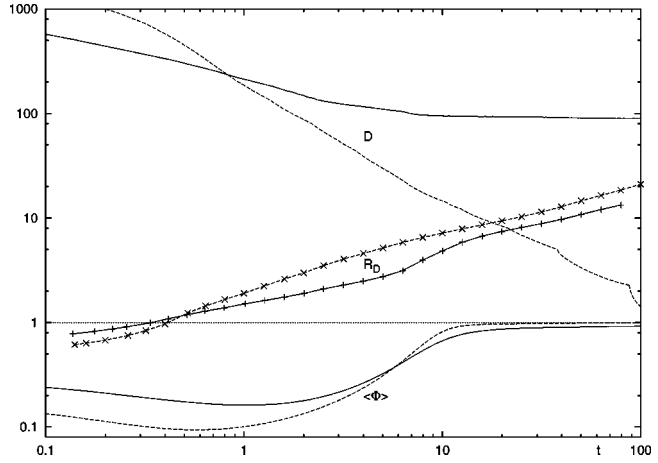

FIG. 3. Comparison of particle numbers D, angular correlation lengths R_D, and the average bag fields $\langle\Phi\rangle$ as functions of time t after a sudden quench, for evolutions under the full model with constraint $B=0$ (full lines), and the pure linear σ model (no fourth-order term, no constraint on B) (dashed lines); (100×100 grid, $l=2$, $\lambda=2$).

stable isolated textures may meet and annihilate as can be observed in Fig. 1 near $t\sim10^4$.

Figure 1 is obtained for B constrained to $B=0$ and for scale $l=2$, such that the resulting bag structures extend only over a few lattice cells. The long-time behavior after the roll down phase is highly sensitive to the size of the developing stable textures, i.e. to the fraction of lattice space occupied by the bags because, evidently, overlapping textures quickly combine or annihilate. Their size is governed by l, and in the range up to $l<5$ the structures created are reasonably isolated. We shall see later that for the point of view of DCC signatures the long-time behavior after the roll down is irrelevant. Defining the typical roll-down time t_{RD} as that point in time when the lattice averaged $\langle\Phi\rangle$ has reached a value of 0.8, we plot in Fig. 2 t_{RD} as function of l and λ, respectively, for 15 events each. For B constrained to $B=0$ the average values follow power laws $t_{RD}\sim l^{2.4}$ and $t_{RD}\sim\lambda^{-1.2}$ with good accuracy. These numerical results show that the roll-down time t_{RD} scales as $(l^2/\lambda)^{1.2}$ which means that it is essentially determined by the potential term $(\Phi^2-1)^2$ alone. It is almost unaffected by the fourth-order derivative term which scales with the product $(l^2\lambda)$, while the second-order gradient terms in U cause only a mild increase of the scaling exponent to the observed value of 1.2.

We interpret the stable textures as baryons floating in the effective meson pion field. Fixing their spatial extent in terms of lattice units through the choice of l provides the physical scale for the lattice constant. We shall typically choose $l=2$ such that baryons carrying one unit of winding number (=baryon number) acquire a radius for their topological density of about two lattice constants. With a typical nucleon radius of 0.6–1.0 fm, for $l=2$, the lattice constant then corresponds to ~0.3–0.5 fm. For an accurate description of the texture and bag profiles of individual baryons such a small value $l=2$ is not really sufficient, as has been discussed in detail in the investigation of static solutions in [13]. But within the present context this aspect is not essential. For physical vacuum boundary conditions this choice also suggests the typical lattice size L, which should be sufficiently large to cover the spatial extent of the high-temperature area after a typical hadronic (heavy-ion) collision. So values of $20<L<100$ seem appropriate, and they are technically easy to handle.

Through Eq. (17) the value of λ is directly tied to the σ mass. For $l=2$ the choice $\lambda=2$ leads to $m_\sigma^2=1$ (in inverse lattice units), which appears quite reasonable, being of the order of a typical baryon mass. In the discussion in [13] we have seen that for $\lambda=2$ the stable textures are confined into the interior of well-developed bag structures which we consider an essential feature of physical baryons. For all these reasons we shall in the following present results mostly for $l=2$ and $\lambda=2$.

In order to obtain the roll-down times for that case we extract from Fig. 2 the values of t_{RD} for this two-dimensional $O(3)$ model

$$t_{RD}\approx6\left(\frac{l^2}{\lambda}\right)^{1.2}. \tag{23}$$

For $l=2$, $\lambda=2$ this is about 14 relaxation time units.

To guide the eye for the increase of the correlation length R_D we have included in Fig. 1 the power law $R=1.3t^{0.5}$ as a straight dashed line. Although there are typical deviations prior and during the roll-down phase it is remarkable that this classical scaling expectation serves well to describe the growth of oriented domains for this rather complicated interplay of forming and stabilizing extended textures and aligning domains. Apparently, the use of this growth law for estimating domain sizes seems justified throughout the whole time period relevant for DCC signatures.

It is interesting to compare these results with the plain linear σ model. For that purpose we omit in Eq. (14) the current-current coupling and follow the evolution without

putting a constraint on the winding number B. Figure 3 shows two events evolving from identical initial configurations on a 100×100 grid with vacuum boundary conditions. After about 200 relaxation time units the unconstrained linear sigma model has lost all particles and antiparticles ($D\rightarrow0$), and the configuration tends towards global alignment in 3-direction. On the other hand, the full model with a fourth-order Skyrme term included and winding number constrained to $B=0$, finally stabilizes solitons with D of the order of 100 particles plus antiparticles. Comparing the growth rates of the angular correlation lengths R_D for both evolutions it may be seen that there is no dramatic difference in the overall growth exponent. Still, it is evident that especially during the roll-down phase the emerging extended stabilizing textures do present an obstacle against the free and unconstrained ordering process such that the average size of the ordered domains in the full model is noticeably smaller than in the plain linear σ-model evolution.

At this point we may add a few remarks concerning the relaxation constant τ which in the TDGL equation (18) we have simply used as a time unit, because no other propagating terms are present. Of course, we could use Eq. (5) instead of Eq. (6) for simulating evolutions of the classical field. Keeping the propagation velocity at $c=1$ the time unit then is set by the lattice constant. A trivial consequence is that all features which reflect the relaxation, like growth rates or saturation times, are scaled with powers of τ. E.g., for sufficiently small τ the roll-down time t_{RD} scales like $1/\tau$. It turns out that for $\tau\sim0.1$ the evolutions resulting from Eqs. (5) and (6) essentially coincide. For $\tau\sim1$ the propagating waves start showing up in the field configurations and cause oscillatory features in (lattice-) averaged quantities without strongly affecting the late-time evolution. For $\tau>2$ oscillations dominate and due to the nonlinear terms stabilization becomes difficult. So, to be on the safe side for use of the TDGL equation (6), τ should be less than 1. Looking once more at Fig. 3, $t_{RD}\sim10$ (in units of τ) implies that for $\tau\sim0.1$ the roll down is completed after travelling waves have passed about 100 lattice units.

V. COOLING TIMES

The assumption of a sudden quench which underlies the ordering features shown in the previous chapter represents that limit for the actual cooling process where the cooling time τ_c (during which the temperature drops from $T/T_c\sim1$ to $T=0$) is much smaller than the relaxation time which governs the evolution of the field configurations. This instantaneous cooling, where the hot initial configuration for $t>0$ is immediately exposed to the zero-temperature $T=0$ effective potential defines the most off-equilibrium scenario which we can study within this model. To weaken this rather drastic assumption we replace it with an appropriate time dependence of the temperature $T(t)$. Then also the temperature dependence $f^2(T)$ in Eq. (16) has to be specified.

The function $f^2(T)$ in principle is determined from loop contributions and their renormalization group resummation in finite-temperature field theory. Perturbative evaluations are restricted to the vicinity of $T=0$; the complete form of $f^2(T)$ depends on the specific model and is not accurately known. Its essential features, however, are a slow decrease from its $T=0$ value $f^2=1$ for $T>0$, followed by a steeper decrease $f^2\rightarrow0$ as T approaches T_c. For the simulations these essentials are sufficient; the specific form (generally in the form of logarithms) is not important. A very convenient ansatz which comprises these basic features in the region $0<T<T_c$ is

$$f^2(T)=[1-(T/T_c)^\alpha]^2 \tag{24}$$

with $\alpha\sim4$, and $f^2(T)=0$ for $T\geqslant T_c$.

A slow cooling scenario can be realized by externally imposing the dependence $T(t)$ of temperature on time. For a linear quench we take

$$T(t)/T_c=1-t/\tau_c \tag{25}$$

with quench time τ_c, and $T=0$ for $t>\tau_c$. A crucial feature of the ordering process is that the early phase prior to the onset of the roll down is dominated by angular aligning driven by the gradient terms in the σ-model part of Eq. (14) while the effective potential for Φ is of only minor importance. As a consequence, the angular ordering up to the onset of the roll down proceeds quite independently of the actual cooling rate, with $\langle\Phi\rangle\ll1$ in any case. This is fortunate because it renders knowledge of the precise form of $T(t)$ and $f^2(T)$ unimportant and we can safely adopt convenient ansaetze like Eqs. (24) and (25).

For a very slow quench $\tau_c\gg\tau$, after this first angular aligning phase, the roll down then only proceeds up to the momentaneous value of f^2, $\langle\Phi\rangle^2\leqslant f^2(T(t))$. Specifically, the stable textures are being created with profiles which correspond to an instantaneous scale

$$\tilde{l}(t)=lf^{-1}(T(t)) \tag{26}$$

as can be seen from rescaling the modulus of the order parameter to $\tilde{\Phi}=\Phi f^{-1}(T(t))$ in Eq. (14). With $f^2(T(t))<1$ the nascent stable objects in the slow quench are much larger than for the sudden quench, i.e. fewer of them survive as separate isolated textures. Subsequently, further ordering proceeds essentially as equilibrium evolution where the stable objects shrink according to $\tilde{l}(t)$ in Eq. (26) until they finally assume their $T=0$ size with accompanying rearrangement of surrounding aligned domains.

As an intermediate case we consider evolutions where the cooling time is comparable with the roll-down time t_{RD} in Eq. (23), conveniently again as linear quench with $\tau_c\sim10$ for $l=2$ and $\lambda=2$. In the very early phase the evolutions closely follow the slow quench with very small $\langle\Phi\rangle$ and a steeper decrease of the particle number D as compared to the sudden quench, but as t approaches τ_c the roll down proceeds rapidly towards the sudden quench value $\langle\Phi\rangle\approx1$, with a corresponding pronounced loss in energy E and a typical increase of R_D. For $t>t_{RD}$ the number of textures with $T=0$ profiles stabilizes at values intermediate between sudden and very slow quench and the angular ordering of aligned vacuum domains proceeds along the classical $t^{0.5}$ law.

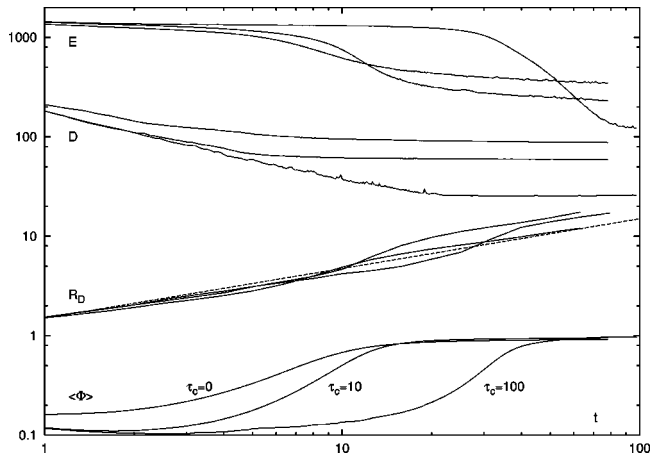

FIG. 4. Energies E, particle numbers D, angular correlation lengths R_D, and average bag fields $\langle\Phi\rangle$ for three events (100×100 grid, $\lambda=2, l=2$) with linear quench (24) and three different cooling times: $\tau_c=0$ (sudden quench), $\tau_c=10$ (intermediate), $\tau_c=100$ (very slow quench). The dashed line indicates the growth law $R_D\sim t^{0.5}$.

Figure 4 shows three typical evolutions with $l=2$ and $\lambda=2$ and a total winding number constrained to $B=0$, starting from the same initial configuration, for $\tau_c=100$ (very slow), $\tau_c=10$ (intermediate), and $\tau_c=0$ (sudden) quench. Figure 5 presents bag contours at $\Phi=0.4,0.6,0.8$ of the stable textures with varying individual winding numbers (summing up to $B=0$) which have been established after $t\sim100$ for these three different cooling rates. It is quite evident from Fig. 4 that the rate of increase of the correlation lengths R_D before and after the roll down ($t\sim10$–20) is unaffected by the cooling rate. Differences in the angular ordering, however, show up in the evolving particle numbers which reflect the changing effective potential through the size of nascent textures.

For these slow quenches which proceed with a finite cooling rate evolutions are subject to fluctuational noise given by the last term in Eq. (18). Its variance depends on the physical nature of the dissipative $\dot{\mathbf{\Phi}}$ term in Eq. (18), i.e., to which extent it originates purely from particle emission, or from kinematical expansion of the spatial volume, or from a heat bath of eliminated high-frequency modes. In any case, its strength according to the fluctuation-dissipation theorem decreases linearly with temperature T. Its general influence on the evolving configurations is very transparent: for finite T it will tend to disturb the ordering process at each time step. This results in a slight decrease of the slopes of those observables which reflect the ordering, specifically the correlation length R_D, the average $\langle\Phi\rangle$, the particle numbers D, the total energy E. On the other hand, fluctuations support (Brownian) motion of nascent textures which combine more easily into larger structures with increased individual winding numbers. So, evolutions subject to noise finally produce increased values of D distributed into larger clusters of positive or negative winding number. Naturally, only very slow quenches are noticeably affected by the noise. For definiteness, the evolutions shown in Fig. 4 are obtained from Eq. (18) with the last term $\boldsymbol{\xi}$ omitted completely. Effectively, the inclusion of noise produces evolutions which resemble those for quenches with slightly reduced quench time.

As we have seen, the physically most relevant characteristic of the ordering evolution is the roll-down time where the bag field Φ approaches within aligned (but still mostly disoriented) domains the momentous value of $f(T)$ and isolated textures are being established near their borders. This important feature is most clearly brought forth for $\tau_c\to0$; therefore, in the following we preferably will consider ordering processes after instantaneous cooling.

VI. EXPLICIT SYMMETRY BREAKING

Explicit symmetry breaking of the global $O(3)$ symmetry is of crucial importance for the ordering process. Its weakest form is imposed through boundary conditions where a specific vacuum orientation, e.g. $\mathbf{\Phi}=(0,0,1)$, along the lattice boundary is enforced. For physical processes this, apparently, is also a most natural condition. With increasing time after a sudden quench the influence of this surrounding vacuum will grow deeper and deeper into the randomly ordering interior and eventually reorient aligned domains along the chosen vacuum direction. Clearly, the strength of this aligning effect depends on the finite size L of the lattice. For L of the order of 100 it does not change the essential features of the evolution. There is only one ordering parameter, the absolute value of the averaged ''direction''

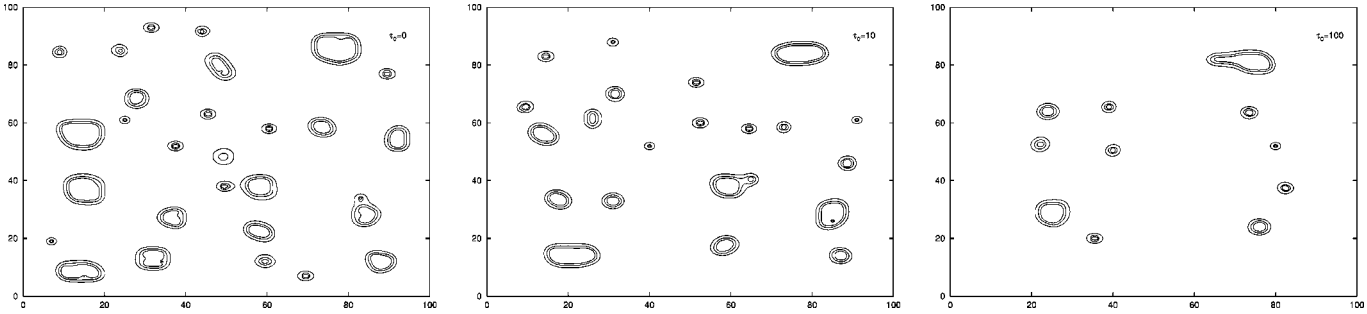

FIG. 5. Bag contours (drawn at $\Phi=0.8,0.6,0.4$ from outside to inside) of isolated baryons remaining at time $t=100$, for the 3 events shown in Fig. 4 which differ by their cooling times $\tau_c=0,10,100$. By the time $t=100$ the temperature has arrived at $T=0$ in all 3 cases, and the baryons approach their $T=0$ sizes and quasistable shapes. The smallest ones carry one unit of winding number. The total winding number is zero in all three cases. The remaining particle numbers (as can be seen from Fig. 4) are $D=95,65,24$ for the cooling times $\tau_c=0,10,100$, respectively.

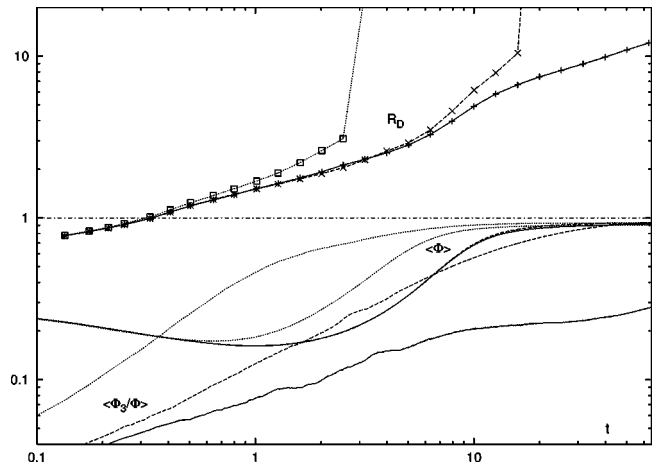

FIG. 6. Angular correlation lengths R_D, average bag fields $\langle\Phi\rangle$, and the averaged 3-component of the field unit vector $\langle\hat{\mathbf{\Phi}}_3\rangle$, for three events ($100\times100$ grid, $\lambda=2$, $l=2$) with different strengths of explicit symmetry breaking, $m_\pi^2=0$ (full lines), $m_\pi^2=0.01$ (dashed lines), $m_\pi^2=0.1$ (dotted lines). [Note that the average bag fields $\langle\Phi\rangle$ for $m_\pi^2=0$ and $m_\pi^2=0.01$ almost coincide.]

$$\langle\hat{\mathbf{\Phi}}\rangle=\sum_{i,j=0}^{L-1}\hat{\mathbf{\Phi}}(i,j)/L^2, \tag{27}$$

which is sensitively affected. For arbitrary periodic boundary conditions this observable remains very small with erratic variations for times long after the roll down, while for the symmetry-breaking vacuum boundary conditions it continually grows in accordance with the growth of the angular correlation length. It is saturated by the averaged 3-component $\langle\hat{\mathbf{\Phi}}_3\rangle$ which carries all of the total $\langle\hat{\mathbf{\Phi}}\rangle$ strength. So, as expected, the oriented domains growing in the vicinity of the boundary contribute coherently to the magnetization and align in the vacuum direction.

Explicit symmetry breaking through a nonvanishing m_π^2 term in Eq. (14) exerts much stronger influence on the ordering process than imposing symmetry-breaking boundary conditions only. We compare in Fig. 6 evolutions under vacuum boundary conditions for values of $m_\pi^2=0.01$, 0.1, and $m_\pi^2=0$. This appears as a reasonable range for pions with a mass of about 10% of the σ mass. For $m_\pi^2=0.01$ the roll down of $\langle\Phi\rangle$ is almost unaffected as compared to $m_\pi^2=0$, while $m_\pi^2=0.1$ accelerates the roll down by a factor of two (with a correspondingly larger number of stable textures created).

Both evolutions with $m_\pi^2\neq0$ show the exponential approach of $\langle\hat{\mathbf{\Phi}}_3\rangle$ to saturation expected for the off-critical quench, in contrast to the unbroken case. (For infinite systems the exponential approach to saturation is governed by $\exp(-2m_\pi^2 t)$ [15].) The saturation value is smaller than one due to the presence of stable textures. In both cases $\langle\hat{\mathbf{\Phi}}\rangle$ is completely saturated by $\langle\hat{\mathbf{\Phi}}_3\rangle$. It may also be noted from Fig. 6 that for $m_\pi^2=0.1$ saturation of $\langle\hat{\mathbf{\Phi}}_3\rangle$ is achieved long before the roll down of $\langle\Phi\rangle$ is completed, while for $m_\pi^2=0.01$ the order is reversed.

It should be noted that the angular correlation function $C(R)$ in the off-critical system approaches $\langle\hat{\mathbf{\Phi}}\rangle^2$ for $R\gg1$. This shows up as an abrupt increase of the half-maximum distance R_D, as soon as the average $\langle\hat{\mathbf{\Phi}}\rangle$ has grown beyond $\sqrt{0.5}\approx70\%$ of its saturation value. Before that sudden increase, R_D already starts to deviate from the growth law of the critical system, because it reflects also the increasing global alignment in 3-direction. So, in the off-critical system, it appears more appropriate to consider only the angular correlations of the transverse ($i=1,2$) components as a measure for the size of disoriented domains.

Additional breaking of the $O(3)$ symmetry occurs through an initial bias in the starting configurations. It originates from the asymmetry introduced into the initial $T>T_c$ ensemble through the $m_\pi^2\Phi_3$ symmetry-breaking term in Eq. (14). It will not alter the exponent of the exponential approach to saturation, but it will reduce the factor in front of the exponential. This causes another considerable reduction of saturation times.

VII. PION EMISSION AS A DCC SIGNATURE

As we discussed in Sec. II signatures of the evolving disoriented domains may be carried in the fractions $f(\pi_i)$ of pion multiplicities of kind i emitted at late time during the ordering process. We will investigate these signatures for an ensemble of events evolving after a sudden quench. We compare results for the plain linear σ model [i.e. omitting the four-derivative current-current coupling in Eq. (14), without constraint on winding number B], with the corresponding evolutions for the full Lagrangian (14), with B constrained to $B=0$, which lead to stabilized solitons floating in the surrounding vacuum. For the parameters in the energy functional we choose $l=2$ and $\lambda=2$, such that the emerging solitons develop deep bags and extend over several lattice cells. With this choice the mass of the ($T=0$) σ fluctuations according to Eq. (17) is $m_\sigma=1$.

Let us at first look at the rates ϵ_i (11) of energy carried away by the field components $i=1,2,3$ for the pure linear σ model with no explicit symmetry breaking, $m_\pi=0$. The direction of spontaneous symmetry breaking then is fixed by the surrounding vacuum alone, which is imposed through the condition that the chiral field is kept at $\mathbf{\Phi}=(0,0,1)$ at all times on the boundary of the lattice. For these events the roll-down phase where the average bag field $\langle\Phi\rangle$ grows from a small value to saturation $\langle\Phi\rangle\approx1$ covers the time interval from $t\approx1$ to $t\approx10$ in units of the relaxation time τ. During this time interval the correlation lengths R_D grow from values near $R_D\approx1$ to $R_D\approx10$. These growth rates are quite independent of the lattice size L, such that the average number of disordered domains by the end of the roll-down phase is of the order of $L^2/(\pi R_D^2)$.

In Fig. 7 we show for some arbitrarily selected individual event the rates ϵ_i of emitted energy for two lattice sizes, $L=30$ and $L=80$. Due to the symmetry breaking effect of the surrounding vacuum, emission into the $i=3$ σ direction dominates the pionic $i=1,2$ emission rates during most of the roll-down phase by one to two orders of magnitude.

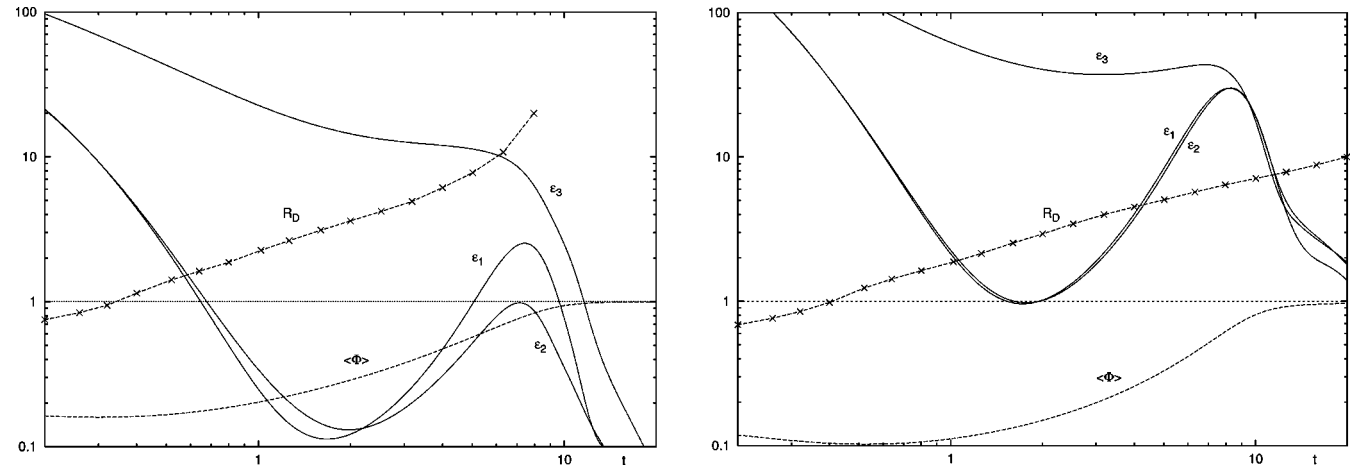

FIG. 7. Angular correlation lengths R_D, average bag fields $\langle\Phi\rangle$, and the rates ϵ_i of energy loss (11) carried by each of the three components $i=1,2,3$ of the chiral field, as functions of time t after a sudden quench, on a 30×30 (left) and an 80×80 (right) grid (plain linear σ model, no constraint on B).

Naturally, this feature is more pronounced in the smaller lattice. Only after completion of the roll down, when the absolute emission rates are getting very small, the average rates become again comparable for $i=1,2,3$. While ϵ_3 is essentially monotonously decreasing during the whole ordering process, the pionic emission occurs in two well-separated pulses. An early, short pulse with high intensity is emitted for times $t<1$ and it is characterized by equipartition $\epsilon_1=\epsilon_2$. This is as expected because at those times the angular correlation lengths R_D are near or less than 1. The second pulse appears during the second half of the roll-down phase; its maximum is at least one order of magnitude smaller than that of the first pulse and it is reached near $\langle\Phi\rangle\approx0.8$. For the larger lattice also this second pulse is characterized by equipartition for both isospin components. However, for the smaller lattice, a significant difference between ϵ_1 and ϵ_2 can be observed. It develops with the onset of the roll down and extends over the whole second pulse of pion emission and thus constitutes a possible DCC signature. Unfortunately, it is just in the small lattice where the pionic signal is strongly dominated by σ emission. (Counting particles instead of energy, this is, however, compensated by the mass ratio.)

It is instructive to analyze the two pion pulses in terms of the TDGL equation (18) which relates (in the pure linear σ model with $m_\pi=0$) $\dot{\Phi}_i$ to $\Delta\Phi_i-(\lambda/l^2)(\Phi^2-f^2)\Phi_i$. As expected, the first pulse is mainly due to the angular ordering effectuated by $\Delta\Phi_i$, while the second pulse is dominated by the potential term. So, the simple approximation $\epsilon_i\sim\langle(\Phi^2-f^2)^2\Phi_i^2\rangle$ provides the essential features of the second maximum (the ''DCC pions''). We may even go further and replace Φ^2 by its lattice average $\langle\Phi^2\rangle$, such that the abundance ratios (13) for DCC pions are approximated by

$$f(\pi_i)\approx\frac{\langle\Phi_i^2\rangle}{\langle\Phi_1^2\rangle+\langle\Phi_2^2\rangle}. \tag{28}$$

In this approximation we recover the commonly used prescription [4] to take the strength of pion emission proportional to the square of the classical field components. (Evidently, this works only for ratios, and only for pions in the second peak.) Based on this approximation, we may derive simple expressions for the probabilities $P_\nu(f)$ to observe in a large ensemble of configurations with ν disoriented domains the ratios $f(\pi_i)$ of DCC pion multiplicities (see the Appendix).

As discussed in Sec. VI, the addition of explicit symmetry breaking through a small pion mass like $m_\pi=0.1$ speeds up the roll-down phase and the aligning of $\mathbf{\Phi}$ into the 3-direction and thus shifts the DCC pions peak to slightly smaller times without affecting the ratios. However, the important difference is that for $m_\pi\neq0$ the emission rate for the 3-component is strongly enhanced relative to the DCC pions, such that also for a large lattice ($L=80$) during and beyond the whole roll-down phase ϵ_3 dominates the DCC pions by more than an order of magnitude (for $m_\pi=0.1$). [For the small lattice ($L=30$) ϵ_3 dominates by two orders of magnitude.]

The fourth-order Skyrme term plays a minor role during these early stages of the ordering process. Its size stabilizing effect for the emerging solitons affects the late stages after completion of the roll down. Still, as we have discussed at the end of Sec. IV, already the emergence of stable extended structures during the roll-down phase presents an obstacle against the growth of large aligned domains and thus it counteracts large differences in the ratios f_1 and f_2 of DCC pions. This becomes apparent by comparing the probability distributions $P(f)$ obtained from a large ensemble of 3000 events on a 30×30 lattice (Fig. 8), for the plain unconstrained linear σ model, and the full model (14) with constraint $B=0$. We sample into 30 bins the ratios $f(\pi_1)$ extracted from 3000 evolutions at the time when $\langle\Phi\rangle$ grows beyond 0.8, which approximately marks the peak in the DCC pions pulse. Comparing with linearly mixed $P_\nu(f)$ taken from Eq. (A5) for two neighboring values of ν, we may conclude that the presence of stable textures increases the average number of disoriented domains present at that point in time (for the fixed lattice size $L=30$) from 2–3 to 4–5. As we have discussed

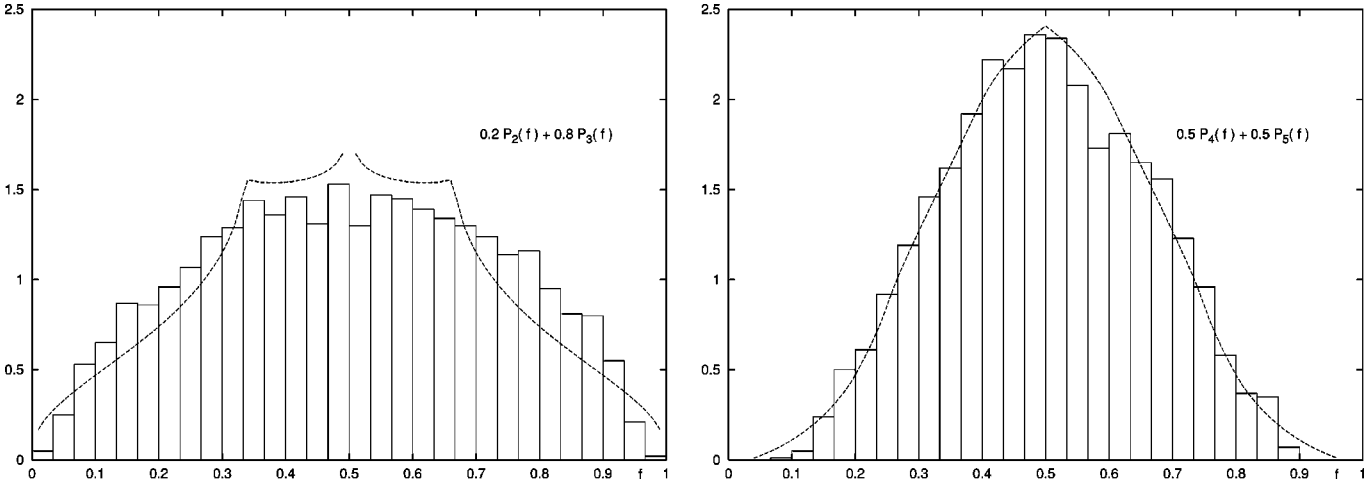

FIG. 8. Probability distributions $P(f)$ for the abundance ratios $f_1(t)$ (13) of DCC pions extracted from an ensemble of 3000 events at roll-down time t_{RD}. For comparison, suitable mixtures of $P_\nu(f)$ selected from the approximation (A5) are shown by the dashed lines. The events evolve after a sudden quench on a 30×30 grid, with no explicit symmetry breaking, according to the plain linear σ model without constraint (left), and for the full model with $B=0$ (right).

above, this average number of ν increases with L^2. Figure 9 shows the corresponding distributions for 3000 events on a $L=60$ lattice. The distribution obtained from the linear σ model is very nicely reproduced by $P_\nu(f)$ with $\nu=13$, while the full and constrained to $B=0$ evolutions are compatible with $\nu=27$, which again shows the strong obstruction of domain growth through the creation of stable textures. Still, it should be remembered that the $P_\nu(f)$ of Eq. (A5) which we use for comparison are derived under the rather poor approximation (28) and the assumption that all domains are of equal size.

To illustrate the influence of the cooling rate for slow quenches Fig. 10 shows two evolutions with cooling time $\tau_c=100$ as discussed in Sec. V. With this choice the cooling time is large as compared to the roll-down time after a sudden quench. The decisive feature of the evolution on a small 30×30 lattice is that the saturation of $\langle\Phi_3\rangle$ is almost completed before the beginning of the roll down of $\langle\Phi\rangle$. Consequently, the DCC pion pulse which still occurs during the late roll-down phase is suppressed by almost four orders of magnitude as compared to σ emission ϵ_3. On this small lattice the disoriented domains show up in the pion emission ratios, while on a larger (80×80) grid, the saturation of $\langle\Phi_3\rangle$ is delayed and the height of the DCC pion pulse increased, but it is characterized by equipartition between ϵ_1 and ϵ_2. So, also in this respect the sudden quench provides the better conditions for a DCC signal.

VIII. CONCLUSION

In this paper we have investigated the phase ordering of a 2D $O(3)$ model under dissipative dynamics. The peculiarity of the underlying Lagrangian is that it stabilizes extended textures through a fourth-order current-current coupling. This is introduced to get an idea how emerging topological solitons with stable sizes interact with the growth of aligned domains. The winding number can be kept fixed to simulate in this model the analogy of baryon number conservation

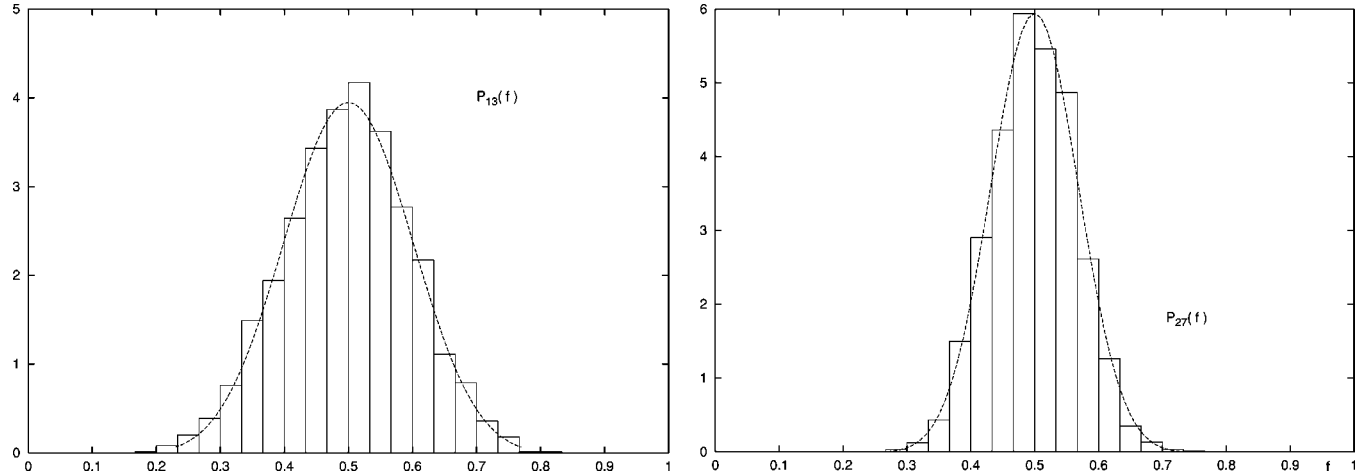

FIG. 9. The same as in Fig. 8, but for a 60×60 grid.

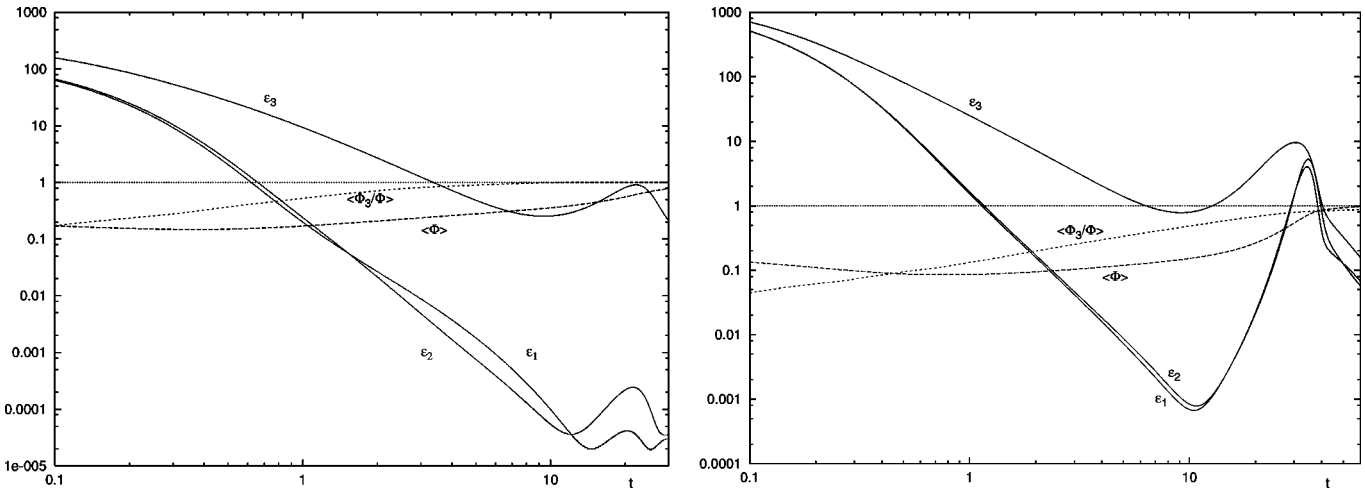

FIG. 10. Average bag fields $\langle\Phi\rangle$, averaged 3-components of the field unit vector $\langle\hat{\mathbf{\Phi}}_3\rangle$, and the rates ϵ_i of energy loss (11) carried by each of the three components $i=1,2,3$ of the chiral field, as functions of time t after a very slow quench ($\tau_c=100$), on a 30×30 (left) and an 80×80 (right) grid (plain linear σ model, no constraint on B).

which is an important feature of models of hadronic systems. Two parameters characterize the model: One fixes the spatial size scale of the stabilized ''baryons,'' the other determines the depth of the bag profile, into which the winding (baryon-) density is confined. Shallow bags correspond basically to the nonlinear version of the model; deep bags realize the unbroken chiral symmetry in the interior of baryons, as it would be expected in hadronic systems.

Apart from studying the influence of different ways of symmetry breaking, and the effects of different quench rates on the ordering observables, we are especially interested in the possibility of finding DCC signatures in the emitted particle radiation. All results are based on the assumption that the relaxation proceeds on a sufficiently slow time scale, such that it provides an adiabatically changing source for the emitted radiation. Therefore its motion is treated classically, and the amount of radiated energy is simply obtained from the classical energy loss of the source. Quantum field-theoretic amplitudes enter only into the relaxation constant τ which, however, has not been determined, but simply used as a time unit for the ordering dynamics.

From the results obtained in this framework we may draw the following conclusions: The classical Allen-Cahn growth law $R_D\sim t^{0.5}$ for disoriented domains is not seriously disturbed by the stabilizing terms in the Lagrangian and the emerging stable textures, although there are characteristic deviations from it during the roll-down phase where the separation into domains of false vacua and deep bags mainly takes place. The factor in front of the $t^{0.5}$ power law, however, is decreased as compared to the pure unconstrained linear σ model, such that the average size of disoriented domains after completion of the roll-down is reduced. The roll down time varies with the two parameters of the model essentially as expected from simple scaling arguments. It represents the crucial characteristic of the ordering process; it is not very sensitive to small explicit symmetry breaking and varies with the quench rate in the expected way. Explicit symmetry breaking strongly affects the saturation time of the average orientation, the factor in front of the exponential approach to saturation depends severely on the (random) initial conditions of each individual event. The number of baryons (plus antibaryons) finally surviving the ordering process is determined by the time of the onset of the roll down. The angular correlation length at that time measures the average distance of regions with high winding density which develop into separate stable structures with an integer winding number during and after the roll-down phase. Therefore slow quenches lead to low baryon density.

The intensities of emitted radiation in our approach is determined by the square of the time derivative of the classical field, averaged over the spatial volume (or area), and not by the square of the classical field itself. This allows us to identify two well-separated radiation pulses for the transverse (''pionic'') components of the chiral field. The later one, emitted towards the end of the roll-down phase carries the signature of the disoriented domains established by that time, so it constitutes the DCC signal. With the growth law of the angular correlations fixed, the average size of disoriented domains at the time of completion of the roll down is also fixed. Therefore the average number of disoriented domains on an $L\times L$ lattice which contribute to the DCC signal increases like L^2, and deviations from equipartition in the intensities carried by the different isospin directions quickly vanish with increasing L. On the other hand, for small L, the pion signal is buried under a large pulse of emission in the longitudinal (σ-) direction, because the explicit symmetry breaking effect of the surrounding true vacuum is strong for small lattice sizes.

The broadening of the probability distributions for the pionic intensity ratios constitutes the DCC signature. We have extracted it from large ensembles of events under the assumption that these pions, emitted at a specific point in time (or averaged over a short time interval near the roll-down time) can be observed separately from the bulk of other pions and σ's emitted. We find that in those cases where a noticeable broadening occurs, the relative amount of energy

carried away in the DCC pulse is suppressed by orders of magnitude. Of course, quantitative statements require knowledge of the parameters in the model, cooling rates, physical size of the lattice as compared to correlation length, baryon size. In the present model, all these conditions remain more or less arbitrary, and we have chosen them at will to illustrate the main features. However, for application to the ordering dynamics of a hadronic chiral $O(4)$ field, we have quite specific ideas about the relevant parameters in the effective actions. The exponent in the classical Allen-Cahn scaling law is the same for (2+1)D O(3) and (3+1)D O(4) models; the homotopy groups $\pi_2(S^2)$ and $\pi_3(S^3)$ are isomorph, both characterized by integer winding numbers. So, apart from differences in dimension-dependent cooling rates and the temperature dependence of the condensate $f(T)$, we do not expect dramatic qualitative differences in the ordering features, and we hope that extending the present considerations to the (3+1)D O(4) model will serve to sharpen our expectations with respect to the observability of DCC signals in hadronic processes.

ACKNOWLEDGMENT

The author appreciates helpful discussions with H. Walliser.

APPENDIX: PROBABILITY DISTRIBUTIONS

Consider a configuration where the classical field is uniformly aligned into some direction, thus forming one single disoriented domain, with the field components ($i=1,2,3$) parametrized as

$$\Phi_{i=1,2,3}=\Phi(\sin\theta\cos\phi,\sin\theta\sin\phi,\cos\theta). \tag{A1}$$

Then, within the approximation (28), we find for the fraction of pions emitted with isospin component $i=1$, relative to the number of all pions ($i=1,2$)

$$f(\pi_1)=\cos^2\phi. \tag{A2}$$

In an ensemble of events where all orientations of $\Phi_{1,2}$ are equally probable the ensemble average $\langle f\rangle$ of $f(\pi_1)$ is, of course, $\langle f\rangle=1/2$. The probability $P(f)$ to find in one event of that ensemble the fraction f (for pions of either kind i) then is obtained from

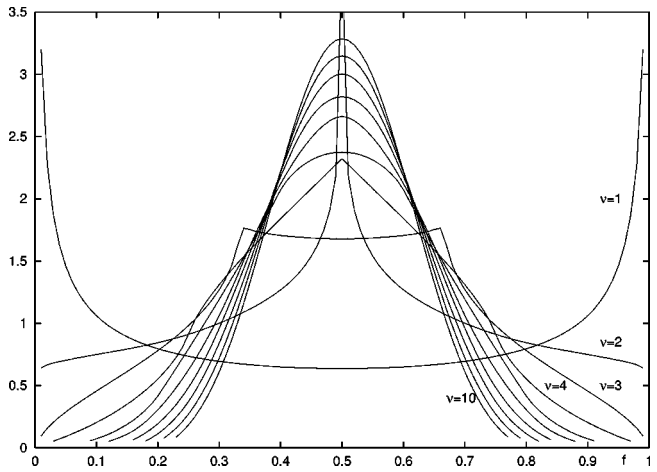

FIG. 11. The probability distributions $P_\nu(f)$ for observing the fraction f of pions with a given isospin component $i=1$ or $i=2$ in an ensemble of configurations with ν disoriented domains of size $1/\nu$, according to Eq. (A5).

$$\langle f\rangle=\frac{1}{2\pi}\int_0^{2\pi} f\,d\phi=\int_0^1 fP(f)\,df \tag{A3}$$

as

$$P(f)=\frac{1}{\pi\sqrt{f(1-f)}}. \tag{A4}$$

[Note the difference to the standard chiral $O(4)$ model, where $P(f)=1/(2\sqrt{f})$.] For ν such domains of size $1/\nu$ the probability $P_\nu(f)$ to find the fraction f in a given event then is

$$P_\nu(f)=\int_0^1\cdots\int_0^1\delta\left(f-\frac{1}{\nu}(f_1+\cdots+f_\nu)\right)\times P(f_1)\cdots P(f_\nu)\,df_1\cdots df_\nu \tag{A5}$$

with $P(f)$ given by Eq. (A4). Some of these functions, for values from $\nu=1$ to $\nu=10$, are shown in Fig. 11. For increasing ν they are, of course, more and more sharply peaked around $f=1/2$.

[1] For a review, see A.J. Bray, Adv. Phys. **43**, 357 (1994).

[2] K. Rajagopal and F. Wilczek, Nucl. Phys. **B404**, 577 (1993); S. Gavin, A. Gocksch, and R.D. Pisarski, Phys. Rev. Lett. **72**, 2143 (1994); G. Amelino-Camelia, J.D. Bjorken, and S.E. Larsson, Phys. Rev. D **56**, 6942 (1997); M. Asakawa, Z. Huang, and X.-N. Wang, Phys. Rev. Lett. **74**, 3126 (1995); A.K. Chaudhuri, hep-ph/0007332; J. Serreau, Phys. Rev. D **63**, 054003 (2001).

[3] D. Boyanovsky, D.-S. Lee, and A. Singh, Phys. Rev. D **48**, 800 (1993); D. Boyanovsky, H.J. de Vega, and R. Holman, *ibid.* **51**, 734 (1995); F. Cooper, Y. Kluger, E. Mottola, and J.P. Paz, *ibid.* **51**, 2377 (1995); M.A. Lampert, J.F. Dawson, and F. Cooper, *ibid.* **54**, 2213 (1996); J. Randrup, Phys. Rev. Lett. **77**, 1226 (1996); Phys. Rev. D **55**, 1188 (1997); Heavy Ion Phys. **9**, 289 (1999); Phys. Rev. C **62**, 064905 (2000).

[4] A.A. Anselm, Phys. Lett. B **217**, 169 (1989); A.A. Anselm and M.G. Ryskin, *ibid.* **266**, 482 (1991); J.P. Blaizot and A. Krzywicki, Phys. Rev. D **46**, 246 (1992); **50**, 442 (1994); Acta Phys. Pol. B **27**, 1687 (1996); J.D. Bjorken, Int. J. Mod. Phys. A **7**, 4189 (1992); Acta Phys. Pol. B **23**, 561 (1992); **28**, 2773 (1997); K.L. Kowalski and C.C. Taylor, SLAC-PUB-92-6; K.L. Kowalski, J.D. Bjorken, and C.C. Taylor, SLAC-PUB-

6109, 1993; S. Gavin, Nucl. Phys. **A590**, 163c (1995).
[5] T.H.R. Skyrme, Proc. R. Soc. London **A260**, 127 (1961); E. Witten, Nucl. Phys. **B223**, 422 (1983).
[6] T.W.B. Kibble, J. Phys. A **9**, 1387 (1976); N.H. Christ, R. Friedberg, and T.D. Lee, Nucl. Phys. **B202**, 89 (1982).
[7] T.A. DeGrand, Phys. Rev. D **30**, 2001 (1984); J. Ellis and H. Kowalski, Phys. Lett. B **214**, 161 (1988); J. Ellis, U. Heinz, and H. Kowalski, *ibid.* **233**, 223 (1989); J. Ellis, M. Karliner, and H. Kowalski, *ibid.* **235**, 341 (1990); J. Dziarmaga and M. Sadzikowski, Phys. Rev. Lett. **82**, 4192 (1999).
[8] M. Asakawa, H. Minakata, and B. Mueller, Phys. Rev. D **58**, 094011 (1998).
[9] T.S. Biro and C. Greiner, Phys. Rev. Lett. **79**, 3138 (1997); Z. Feng, D. Molnar, and L.P. Csernai, Heavy Ion Phys. **5**, 127 (1997).
[10] A.D. Rutenberg, Phys. Rev. E **51**, R2715 (1995); M. Zapotocky and W.J. Zakrzewski, *ibid.* **51**, R5189 (1995); A.D. Rutenberg, W.J. Zakrzewski, and M. Zapotocky, Europhys. Lett. **39**, 49 (1997); G.J. Stephens, Phys. Rev. D **61**, 085002 (2000).
[11] S.L. Sondhi, A. Karlhede, S.A. Kivelson, and E.H. Rezayi, Phys. Rev. B **47**, 16 419 (1993).
[12] G. Holzwarth, Nucl. Phys. **A672**, 167 (2000).
[13] G. Holzwarth and J. Klomfass, Phys. Rev. D **63**, 025021 (2001).
[14] S.M. Allen and J.W. Cahn, Acta Metall. **27**, 1085 (1979).
[15] J.A.N. Filipe, A.J. Bray, and S. Puri, Phys. Rev. E **52**, 6082 (1995).